Journal of
Manufacturing and Materials Processing

MDPI

Article

Modeling of Drag Finishing—Influence of Abrasive Media Shape

Irati Malkorra [1,2,*], Hanène Souli [2], Ferdinando Salvatore [2], Pedro Arrazola [3], Joel Rech [2], Mehmet Cici [2], Aude Mathis [4] and Jason Rolet [1]

1 IRT-M2P, 4 Rue Augustin Fresnel, 57070 Metz, France; Jason.ROLET@irt-m2p.fr
2 Ecole Centrale de Lyon-ENISE, University of Lyon, LTDS CNRS UMR 5513, 58 Rue Jean Parot, 42000 Saint-Etienne, France; hanene.souli@enise.fr (H.S.); ferdinando.salvatore@enise.fr (F.S.); joel.rech@enise.fr (J.R.); mehmet.cici@enise.fr (M.C.)
3 Faculty of Engineering, Mondragon University, Loramendi 4, 2500 Arrasate, Spain; pjarrazola@mondragon.edu
4 Naval Group, CESMAN, Technocampus Ocean, 5 Rue de l'Halbrane, 44340 Bouguenais, France; aude.mathis@naval-group.com
* Correspondence: irati.malkorra@irt-m2p.fr

Abstract: Drag finishing is a widely used superfinishing technique in the industry to polish parts under the action of abrasive media combined with an active surrounding liquid. However, the understanding of this process is not complete. It is known that pyramidal abrasive media are more prone to rapidly improving the surface roughness compared to spherical ones. Thus, this paper aims to model how the shape of abrasive media (spherical vs. pyramidal) influences the material removal mechanisms at the interface. An Arbitrary Lagrangian–Eulerian model of drag finishing is proposed with the purpose of estimating the mechanical loadings (normal stress, shear stress) induced by both abrasive media at the interface. The rheological behavior of both abrasive slurries (media and liquid) has been characterized by means of a Casagrande direct shear test. In parallel, experimental drag finishing tests were carried out with both media to quantify the drag forces. The correlation between the numerical and experimental drag forces highlights that the abrasive media with a pyramidal shape exhibits a higher shear resistance, and this is responsible for inducing higher mechanical loadings on the surfaces and, through this, for a faster decrease of the surface roughness.

Keywords: drag finishing; numerical modeling; arbitrary Lagrangian–Eulerian (ALE) formulation; abrasive media shape; rheological behavior

Citation: Malkorra, I.; Souli, H.; Salvatore, F.; Arrazola, P.; Rech, J.; Cici, M.; Mathis, A.; Rolet, J. Modeling of Drag Finishing —Influence of Abrasive Media Shape. *J. Manuf. Mater. Process.* **2021**, *5*, 41. https://doi.org/10.3390/jmmp5020041

Academic Editor: Johan Berglund

Received: 23 March 2021
Accepted: 20 April 2021
Published: 26 April 2021

1. Introduction

Drag finishing is a superfinishing process leading to great improvements of surface roughness. Parts are dragged through a slurry composed of a high number of ceramic particles (called 'media') that contain abrasive grains and of an active liquid surrounding them. The interaction between the media and the surface to polish induce either the plastic deformation of roughness peaks or generates microchips [1]. The efficiency of the process depends on several parameters like the drag velocity, which is related to the kinetic energy involved in the contact [2]. A higher velocity is supposed to induce higher contact forces and thus faster surface roughness reduction rates. The type of liquid (water, lubricant, chemical accelerators ...) is also known to influence the surface finish [2–4], since it changes the tribological conditions in the contacts, evacuates media and part debris, and can even accelerate the process thanks to a chemical reaction. However, the dominant factor influencing the final signature of the process is the composition and the geometry of media [5]. Large media are well known as being able to increase contact forces, leading to a faster decrease of surface roughness [6]. It was shown by [7] that the abrasive capacity of media influences material removal rates. However, the drag forces that media induce

when the part is moved through them may also play an important role: higher stresses will result in more material removal and plastic deformation. Up to now, nobody investigated this parameter.

Regarding the effect of the abrasive media shape, two hypotheses are proposed:

- The geometrical contact between media and the surface to polish will define the efficiency of the process. For instance, spherical media are more prone to induce the plastic deformation of roughness peaks, whereas pyramidal media are more likely to generate microchips due to their sharp edges. The material removal rate with this last will be higher.
- The mechanical behavior of the slurry composed by the media and liquid will influence the efficiency of the process. The slurry behaves like a viscous dense liquid at a macroscopic scale. This viscosity, linked to the shear resistance of the slurry, may change with the shape of the particles due to the interlocking between particles [8]. Thus, triangular media may exhibit a higher flow stress, and thus a higher mechanical loading in the contacts and, as a consequence, a higher surface modification.

Experimental investigations are not sufficient to prove these hypotheses. Thus, some researchers have proposed numerical models to bring some scientific explanations. On the one hand, Discrete Elements Methods (DEM) model the interaction between a large number of particles and a solid. Their application in drag finishing by [9,10] exhibits strong limitations, not only in terms of its high computational costs but also the complexity of modeling nonspherical media [11]. On the other hand, some researchers proposed to model a volume of abrasive media as a continuum material. Based on this assumption, Eulerian and ALE (Arbitrary Lagrangian–Eulerian) formulations are employed to model the flow of media [12]. With this type of formulation, computational costs become reasonable [13–16]. However, the identification of the corresponding shear strength for each media remains an issue.

This paper aims to understand the influence of the media shape (sphere and pyramid) on the induced drag forces and the mechanical loading at the interface between abrasive media and the part surface, in order to explain why pyramidal media are more efficient in decreasing surface roughness. To that aim, a 2D ALE (Arbitrary Lagrangian–Eulerian) numerical model is proposed to simulate the flow of media around a cylindrical part surface. The shear resistance of both media is identified thanks to a Casagrande direct shear cell, commonly used in the field of soil mechanics. In parallel, experimental drag finishing tests are performed to estimate drag forces and to follow the evolution of the surface roughness (*Sa*) over time.

2. Experimental Tests

2.1. Materials and Methods

Drag finishing tests have been performed on cylindrical samples made of Inconel 718 (See composition in Table 1 [17]). Two different abrasive media (Figure 1b) were involved: a spherical media of 1 mm in diameter and a pyramidal media of 2 × 2 mm. Regarding the size of the media, the ones that were most similar were chosen. Their size differs by ≈1 mm, and even if it is known that the size of media plays an important role in the efficiency of the process, the influence of the shape is much higher [8]. Both media were composed by abrasive grains and a ceramic bonder.

Table 1. Chemical composition of Inconel 718 (% wt) [17].

Ni	Cr	Fe	Mo	Nb	Ti	Al
53.17	18.41	18.45	2.91	5.51	0.99	0.56

The experimental setup presented by Malkorra et al. [18] has been employed for the tests (Figure 1a). It consists in a modified drag finishing machine. The rotation of the part around its axis was suppressed by equaling the rotation speed of the machine and the one

of the part. Thus, the media flow remains in contact with the same area during the test (Figure 1c). For example, the surface that is referenced as '0°' is submitted to a permanent orthogonal flow of media (at v =1 m/s), whereas the surface referenced as '90°' is submitted to a tangential flow of media. Salvatore et al. [9] showed that the evolution of surface roughness varies for each position around the cylindrical part as the corresponding normal and tangential stresses varies. This configuration, patented by Grange et al. [19], enables one to cover a range of normal stresses and velocities. Indeed, in the frontal area (0°), the normal stress is at a maximum and the sliding velocity is limited. On the contrary, in the lateral area (90°), the normal stress is limited and the sliding velocity is at a maximum. In addition to this, the intensity of the normal and shear stresses at the interface depends strongly on the shear resistance of the slurry.

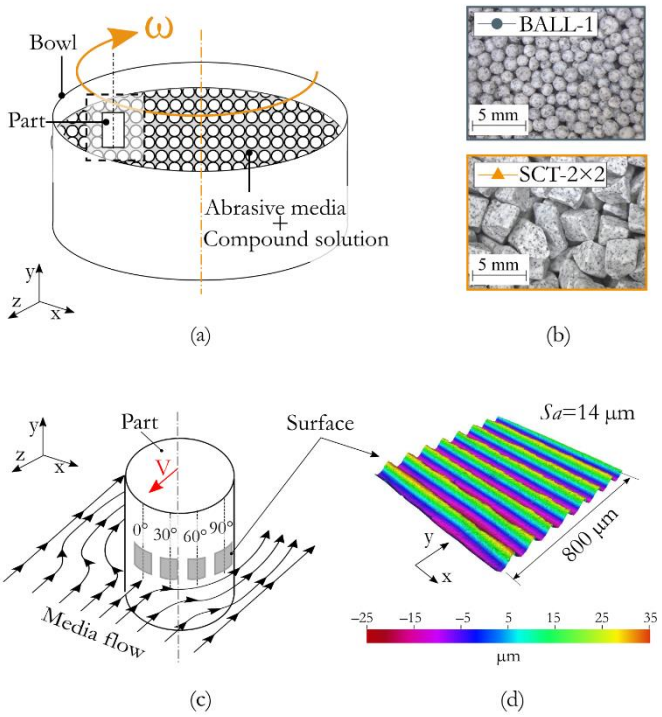

Figure 1. (**a**) Experimental setup, (**b**) abrasive media, (**c**) media flow around the sample and (**d**) surface topography before drag finishing.

During the tests, four areas were analyzed, starting from the frontal zone at 0°, and then at 30°, 60° and 90° degrees (Figure 1c). All initial surfaces presented a periodical topography with a surface roughness of Sa = 14 ± 0.5 µm (Figure 1d) coming from the same manufacturing process developed in [18]. The actual research was carried out in the context of a project dealing with the post-processing of additive manufacturing (AM) parts. For this reason, very rough surfaces are used in the actual work.

The surface roughness evolution was followed up during the tests by means of a focus variation microscope "ALICONA Infinite Focus" with a magnification of 20×, a vertical resolution of 0.1 µm and a lateral resolution of 2.5 µm. The analysis of the measured surfaces (1.5 × 1.5 mm) has been conducted thanks to the Mountain Maps® software. No Gaussian filters were applied in the calculation of the Sa parameter [20].

During the drag finishing tests, the drag forces have been measured in the experimental setup shown in Figure 2a. The workpiece was dragged through the media that were placed in a large box, the black arrows show (1) the forward and (2) return directions). The resultant force (Fy (exp.)) applied on the workpiece was tracked, as shown in Figure 2b. Only the forces measured in the first direction (1) in Figure 2b were taken into account.

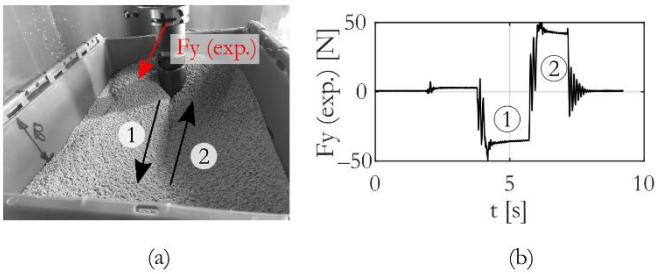

Figure 2. (**a**) The experimental setup for measuring the drag forces (Fy (exp.)) and (**b**) the resultant force signal.

2.2. Results

Figure 3 shows the evolution of the *Sa* parameter corresponding to the four areas. It can be observed that:

- The *Sa* reduction is faster with the pyramidal media than with the spherical ones. For example, at 0°, after 120 min, the *Sa* reductions for the pyramidal and spherical media are respectively 93% and 26%.
- The *Sa* reduction is greater at 0° than at 90° in the case of the pyramidal media, with 93% and 40%, respectively. However, the roughness evolution is similar for all the surface angles for the spherical ones, with an *Sa* reduction between 23–35%.
- Regarding the measured drag forces (Fy (exp.)), the pyramidal media lead to a higher force compared to the spherical ones (71 N and 37 N, respectively).

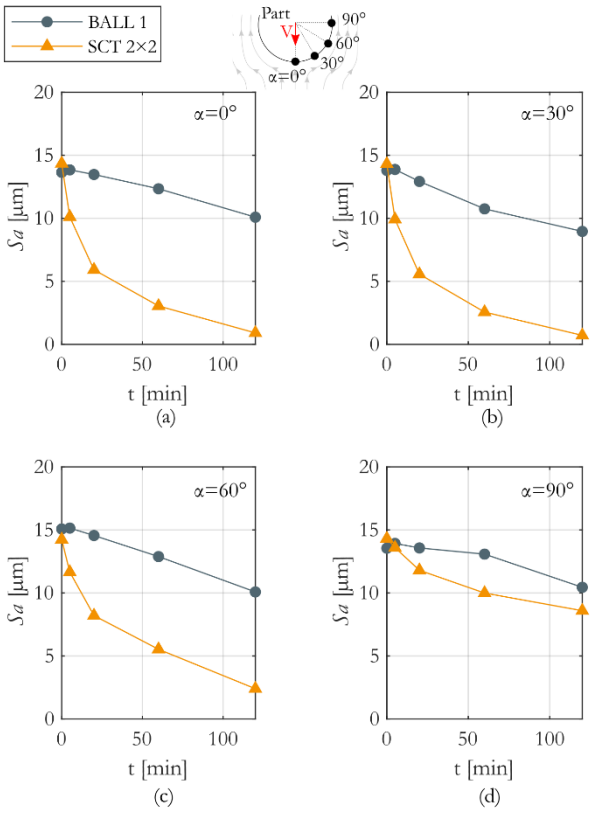

Figure 3. Drag finishing experimental results: *Sa* evolution according to the orientation angle (α) (**a**–**d**) of the surface and the abrasive media (BALL 1 and SCT 2 × 2).

3. The Numerical Model

In order to reach a better understanding of the experimental results, a numerical model that simulated the flow of abrasive media around the cylindrical part was developed.

A 2D model based on an Arbitrary Lagrangian–Eulerian (ALE) [12] formulation was employed in order to simulate the media flow around the part thanks to the commercial code Abaqus/Explicit©. The model has two parts (Figure 4):

- The "Workpiece": defined as a rigid body and fixed in its axis. It is considered that the deformations in the workpiece are negligible in comparison to those in the abrasive media flow.
- The abrasive "Media": defined as a deformable body, the mesh is fixed and the material flows through it thanks to an ALE formulation. The entrance and exit surfaces of the material are defined as Eulerian surfaces (Figure 4).

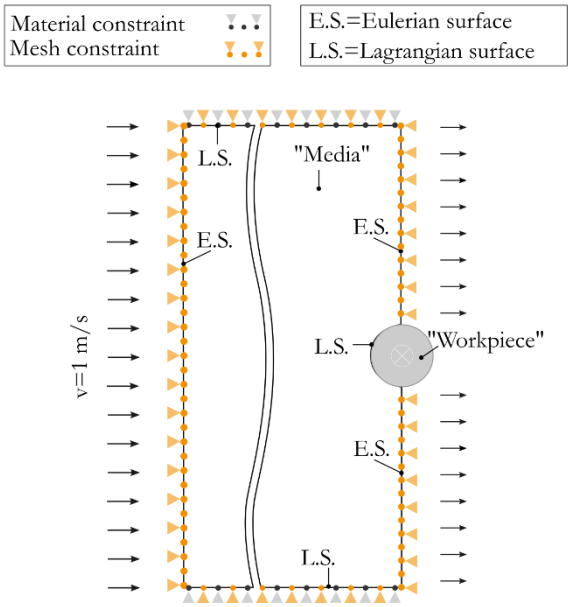

Figure 4. Schematic figure of the numerical model.

At the interface between the two parts, a constant Coulomb friction coefficient (μ) of 0.25 was applied [21]. The friction coefficient is the proportionality coefficient between normal and tangential forces between two solids in contact. A kinematic contact algorithm was employed with a finite sliding formulation. Both parts were meshed uniformly with 4-node plane strain elements (CPE4R) having a size of around 0.98 mm.

3.1. Flow Stress Model of Media

A volume with a high number of media can be considered as granular material and can be modeled as a continuum material based on the techniques and theories commonly used to model soils [8].

The density of the volume of the media was measured, and the elastic properties were extracted from the literature [13] (ρ = 1587 kg/m^3, E = 200 kPa, ν = 0.3). The flow stress or the shear resistance of both slurries was identified thanks to a direct shear cell by Casagrande [8] (Figure 5a). This test relates the normal and tangential stress applied to the cell and gives the internal friction angle of the material. This friction angle is composed of the local friction between particle surfaces (μ) and the contribution of the interlocking (β) between particles due to their shape (Equation (1)).

$$\varphi = \mu + \beta \quad (1)$$

The cell (60 × 60 × 15 mm) was filled by a volume of the slurry, and a uniaxial vertical force was applied (F_y). Then, a velocity (v = 1.27 mm/min) is imposed to the upper part of the cell in order to shear the material (Figure 5b). During the test, the shear stresses (τ) and

the displacement (ε_x) of the cell are followed. As shown in Figure 5c, for each media, three tests with three different uniaxial forces (F_y) were carried out (500, 1000 and 1500 N).

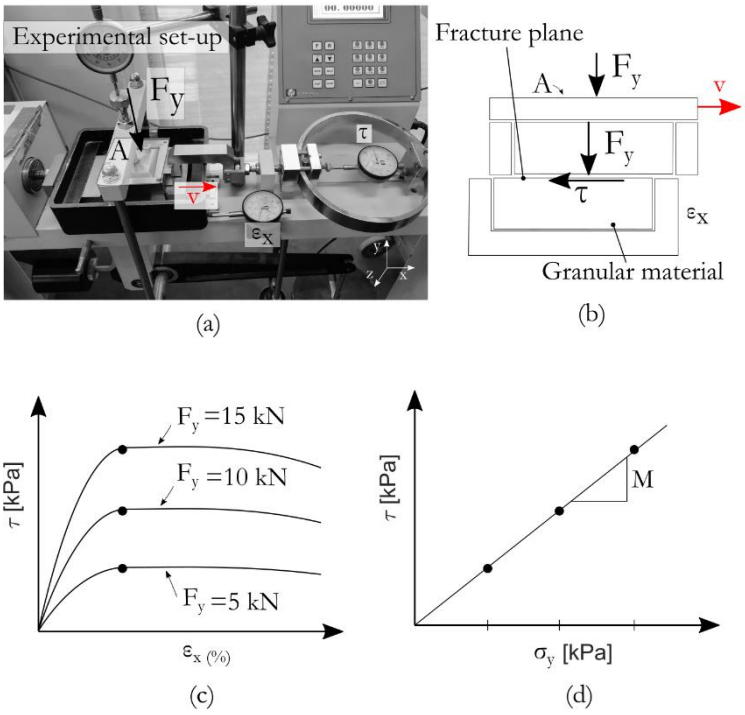

Figure 5. (**a**)The direct shear cell, (**b**) the schematic illustration, (**c**) typical representation of shear test results and (**d**) friction angle calculation procedure.

The maximum shear stress of each curve is chosen (Figure 5c) and plotted in the Mohr's circle (Figure 5d). The slope (M) of the line that links the three points defines the angle of internal friction of the material (φ) (Equation (2)). Figure 6 plots the two lines for both media. It appears that the spherical media presents an angle of $\varphi_{BALL\text{-}1} = 30°$, whereas the pyramidal media leads to $\varphi_{SCT\text{-}2\times2} = 49°$. It was assumed that the local friction angle (μ) was the same for both media, so the difference between the friction angles was due to high interlocking (β) forces between pyramidal particles. In other words, sliding between particles is more difficult due to their pyramidal shape, whereas spherical particles slide easily and present a lower shear resistance.

$$M = \tan(\varphi) \tag{2}$$

A linear Drucker–Prager plasticity model [22,23] was employed to define the material plastic behavior, which is typically used for soil modeling. This yield criterion is written in terms of stress invariants (Equation (3)), where t_{triax} is expressed as in (Equation (4)) and enables one to have different yield values in triaxial tension and compression. p is the equivalent pressure stress, φ is the internal friction angle, and d is the cohesion of the material. The employed granular material is considered as cohesionless, so d was 0. For Equation (4), q was the Mises equivalent stress, K the ratio of the yield stress in triaxial tension to triaxial compression (K = 0.8), and r was the third invariant of the deviatoric stress [22].

$$F = t_{triax} - p\tan\varphi - d \tag{3}$$

$$t_{triax} = \frac{1}{2}q\left[1 + \frac{1}{K} - \left(1 - \frac{1}{K}\right)\left(\frac{r}{q}\right)^3\right] \tag{4}$$

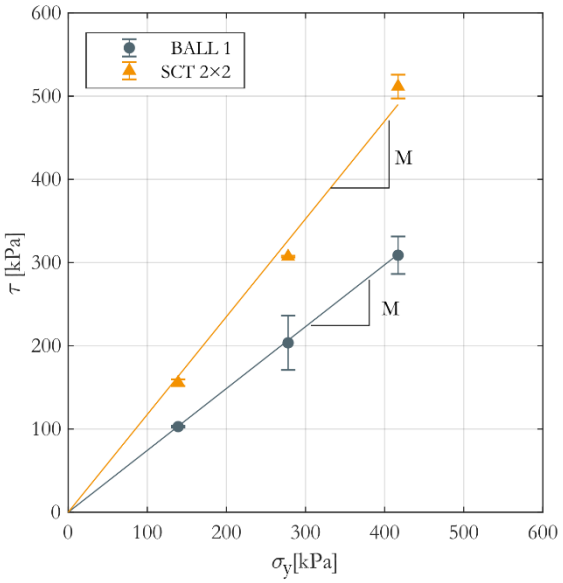

Figure 6. Failure envelopes for both abrasive media.

3.2. Results

The numerical model provides the drag force (Fy (num.) in Figure 7c). Its value is plotted in Figure 7b together with the experimentally measured values (Fy (exp.)) in Section 2.2.

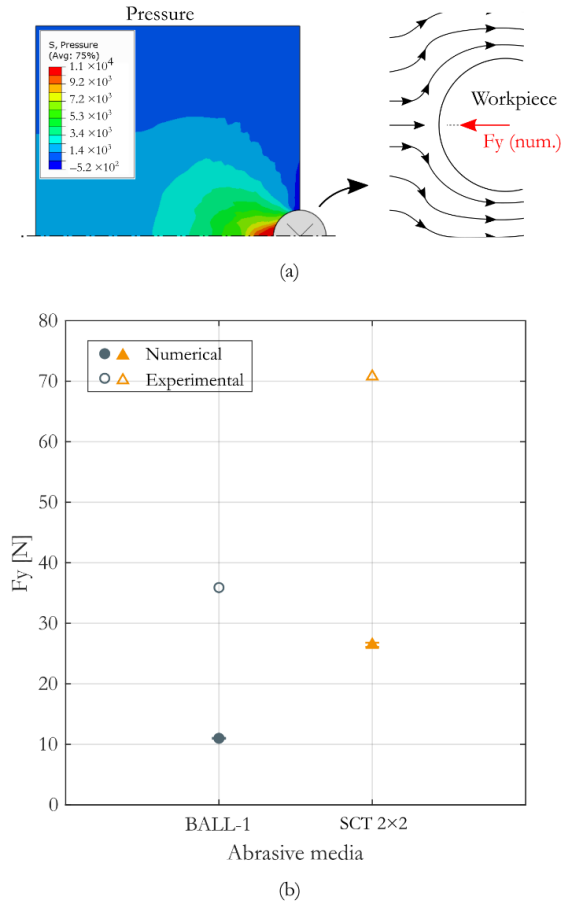

Figure 7. (**a**) The numerical force calculation and (**b**) the comparison between numerical and experimental forces for each media.

The drag forces predicted by the numerical model and the drag forces measured experimentally reveal that the pyramidal media lead to a higher drag force than the spherical ones. There is a big difference between the experimental and numerical values for both media, which means that improvements of the model are necessary to predict more accurate values. However, the trend is similar, and it can be concluded that the model is very sensitive to the flow stress of the granular material.

As a consequence, this enables one to make a qualitative comparison of the stresses induced by each media on the surface of the part, so as to understand why a better and faster surface finish is obtained with the pyramidal media. Figure 8 shows the distribution for each node of the normal stress σ_n and shear stress τ induced around the cylindrical workpiece surface in the case of both abrasive media. In addition, a trend line is also plotted for each cloud. It can be observed that:

- Both the normal stress σ_n and shear stress τ are higher with the pyramidal media. This observation is the direct consequence of the flow stress through the difference of the internal friction angle ($\varphi_{SCT\text{-}2\times2} = 49°$ and $\varphi_{BALL\text{-}1} = 30°$).
- The stress distribution depends on the orientation angle of the surface. At 0°, there is a stagnation point of the media flow, where the normal stresses reach the maximum value. On the contrary, the shear stress is rather high, but somewhat under the values some degrees further. Outside of this stagnation area, the shear stress exhibits a peak of intensity. This peak is wide for the spherical media (between 5–30°), whereas it is narrower for the pyramidal one (between 5–10°). Then, both stresses decrease when increasing the orientation angle until reaching 90°, where their values are minimum.

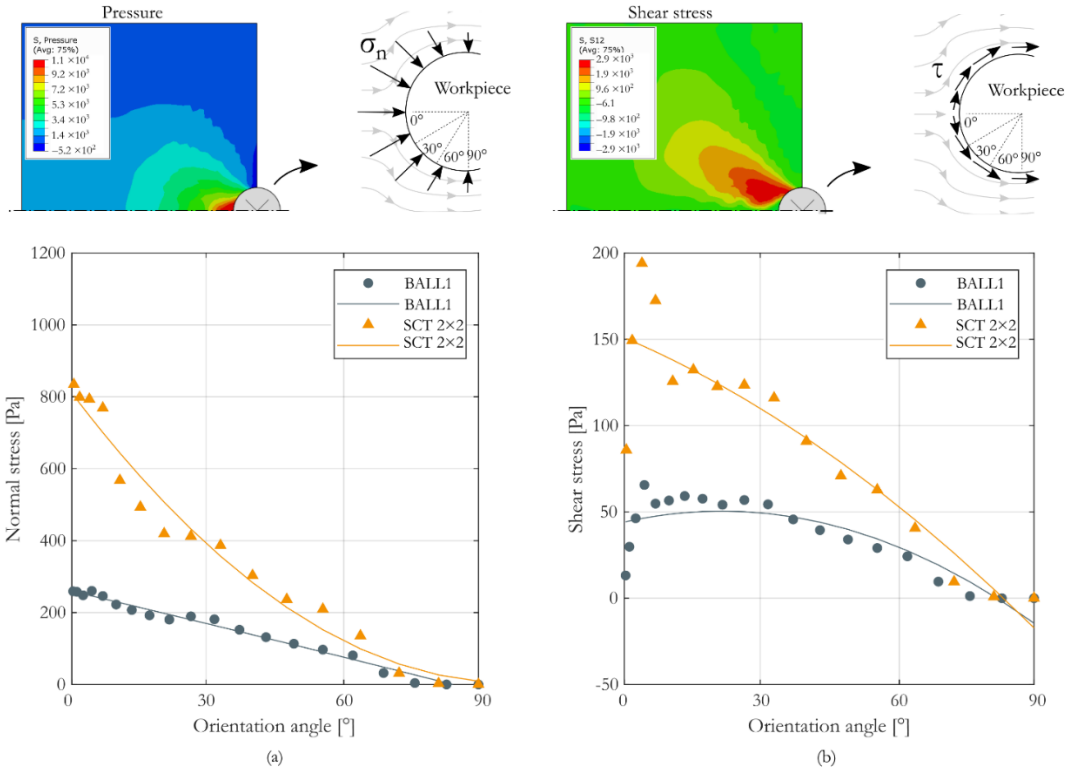

Figure 8. (**a**) Normal stress and (**b**) shear stress depending on the surface orientation angle for both abrasive media.

4. Discussion

The experimental tests demonstrated the efficiency of the pyramidal media to rapidly decrease the surface roughness of parts. This can be correlated with the high shear resistance and the high friction angle (due to the interlocking between individual particles) exhibited by the pyramidal media. This physical parameter of the material induces higher

drag forces in the part, as well as higher normal and shear stresses around its surface. As a consequence, the roughness reduction is faster than with the spherical media.

Due to the variation of both the normal and shear stresses along the workpiece surface, the roughness reduction in each area will also vary. This was reflected in the experimental tests: a different roughness evolution was observed for each surface orientation angle in the case of the pyramidal media.

However, it is remarkable that the evolution of the surface roughness in the case of the spherical media is not strongly influenced by the surface orientation angle. At $\alpha = 30°$, the *Sa* reduction at t = 120 min is slightly higher than for the other angles. This matches with the strongest shear stress value calculated numerically at the same orientation angle.

5. Conclusions

In this paper, experimental drag finishing tests were performed in order to investigate the efficiency of pyramidal and spherical media in reducing the surface roughness on Inconel 718 parts.

It was observed that the pyramidal media was more efficient than the spherical one. In addition, it was stated that the roughness reduction was not uniform all along the part surface. This uniformity is related to the angle of orientation of the surface regarding the media flow. The polishing with the pyramidal media is more sensitive to the orientation angle than with the spherical ones.

With the purpose of understanding the previous experimental observations, a 2D ALE numerical model was developed. This model simulates the flow of media around the cylindrical part. The characterization of the shear strength of each media was done with the Casagrande shear test method, commonly used in civil engineering. Each media presented a different internal friction angle: pyramidal ones presented a higher value due to the contribution of the interlocking between particles.

The model provided a qualitative understanding of the drag finishing process. It was demonstrated that the internal friction angle of the material was directly related to the induced mechanical loadings in the interface and thus to the effectivity of the process. Pyramidal media induce a higher mechanical loading. On the contrary, spherical media induce lower loadings, and the roughness improvement is therefore slower.

Author Contributions: I.M.: Conceptualization, methodology, software, experimental investigation, formal analysis, writing—original draft preparation. H.S.: Methodology, resources, supervision. F.S. and P.A.: Conceptualization, methodology, formal analysis, supervision. J.R. (Joel Rech): Conceptualization, methodology, formal analysis, supervision, writing—review and editing. M.C.: Resources. A.M. and J.R. (Jason Rolet): supervision, project administration. All authors have read and agreed to the published version of the manuscript.

Funding: This research received no external funding.

Data Availability Statement: The data presented in this study are available on request from the corresponding author. The data are not publicly available due to privacy.

Acknowledgments: The authors would like to thank IRT-M2P and the AFTER ALM project partners for the financial support. C. Claudin and H. Seux from the ENISE are thanked for the development of both experimental setups and sample fabrication. G. Methon is thanked for the support in numerical simulation.

Conflicts of Interest: The authors declare no conflict of interest.

Abbreviations

Symbol	Definition
v	Velocity of the abrasive media [m/s]
α	Surface orientation regarding the media flow [°]
Sa	Surface roughness [µm]
t	Time [min]
Fy (exp.)	Experimental drag force [N]
μ	Friction coefficient [-]
ρ	Media density [kg/m^3]
E	Young Modulus [Pa]
ν	Poisson's ratio [-]
β	Interlocking between particles [-]
F_y	Uniaxial vertical force [N]
σ_y	Uniaxial vertical stress [Pa]
τ	Shear stress [Pa]
ε_x	Displacement in x [%]
M	Slope of the yield limit [°]
φ	Internal friction angle [°]
t_{triax}	Term that provides a noncircular yield surface [Pa]
p	Equivalent pressure [Pa]
d	Cohesion [-]
q	Mises equivalent stress [Pa]
K	Ratio between the yield stress in triaxial tension to triaxial compression [-]
r	Third stress invariant [Pa]
Fy (num.)	Numerical drag force [N]
σ_n	Normal stress [Pa]

References

1. Hashimoto, F.; Chaudhari, R.G.; Melkote, S.N. Characteristics and Performance of Surfaces Created by Various Finishing Methods. *Procedia CIRP* **2016**, *45*, 1–6. [CrossRef]
2. Barletta, M.; Pietrobono, F.; Rubino, G.; Tagliaferri, V. Drag finishing of sensitive workpieces with fluidized abrasives. *J. Manuf. Process.* **2014**, *16*, 494–502. [CrossRef]
3. Ciampini, D.; Papini, M.; Spelt, J.K. Impact velocity measurement of media in a vibratory finisher. *J. Mater. Process. Technol.* **2007**, *183*, 347–357. [CrossRef]
4. Mediratta, R.; Ahluwalia, K.; Yeo, S.H. State-of-the-art on vibratory finishing in the aviation industry: An industrial and academic perspective. *Int. J. Adv. Manuf. Technol.* **2015**, *85*, 415–429. [CrossRef]
5. Malkorra, I.; Salvatore, F.; Arrazola, P.; Rech, J. The influence of the process parameters of drag finishing on the surface topography of aluminium samples. *CIRP J. Manuf. Sci. Technol.* **2020**, *31*, 200–209. [CrossRef]
6. Song, X.; Chaudhari, R.; Hashimoto, F. Experimental Investigation of Vibratory Finishing Process. *MSEC* **2014**, *2*, MSEC2014–MSEC4093.
7. Uhlmann, E.; Dethlefs, A.; Eulitz, A. Investigation of material removal and surface topography formation in vibratory finishing. *Procedia CIRP* **2014**, *14*, 25–30. [CrossRef]
8. Das, B.M. *Advanced Soil Mechanics*, 3rd ed.; Taylor & Francis: Boca Raton, FL, USA, 2008. [CrossRef]
9. Salvatore, F.; Grange, F.; Kaminski, R.; Claudin, C.; Kermouche, G.; Rech, J.; Texier, A. Experimental and Numerical Study of Media Action During Tribofinishing in the Case of SLM Titanium Parts. *Procedia CIRP* **2017**, *58*, 451–456. [CrossRef]
10. Uhlmann, E.; Eulitz, A.; Dethlefs, A. Discrete Element Modelling of Drag Finishing. *Procedia CIRP* **2015**, *31*, 369–374. [CrossRef]
11. Li, X.; Li, W.; Yang, S.; Hao, Z.; Shi, H. Study on polyurethane media for mass finishing process: Dynamic characteristics and performance. *Int. J. Mech. Sci.* **2018**, *138–139*, 250–261. [CrossRef]
12. Donea, J.; Huerta, A.; Ponthot, J.-P.; Rodríguez-Ferran, A. Arbitrary Lagrangian-Eulerian Methods. In *The Encyclopedia of Computational Mechanics*, 2nd ed.; Stein, E., Borst, R., Hughes, T.J.R., Eds.; Wiley Online Library: Hoboken, NJ, USA, 2017; Volume 1, Chapter 14; pp. 413–437. [CrossRef]
13. Hashemnia, K.; Spelt, J.K. Finite element continuum modeling of vibrationally-fluidized granular flows. *Chem. Eng. Sci.* **2015**, *129*, 91–105. [CrossRef]
14. Cariapa, V.; Park, H.; Kim, J.; Cheng, C.; Evaristo, A. Development of a metal removal model using spherical ceramic media in a centrifugal disk mass finishing machine. *Int. J. Adv. Manuf. Technol.* **2008**, *39*, 92–106. [CrossRef]
15. Zheng, Q.J.; Yu, A.B. Modelling the granular flow in a rotating drum by the Eulerian finite element method. *Powder Technol.* **2015**, *286*, 361–370. [CrossRef]

16. Huang, A.N.; Kuo, H.P. CFD simulation of particle segregation in a rotating drum. Part I: Eulerian solid phase kinetic viscosity. *Adv. Powder Technol.* **2017**, *28*, 2094–2101. [CrossRef]
17. Chaabani, S.; Arrazola, P.; Ayed, Y.; Madariaga, A.; Tidu, A.; Germain, G. Comparison between cryogenic coolants effect on tool wear and surface integrity in finishing turning of Inconel 718. *J. Mater. Process. Technol.* **2020**, *285*, 116780. [CrossRef]
18. Malkorra, I.; Salvatore, F.; Rech, J.; Arrazola, P.; Tardelli, J.; Mathis, A. Influence of lubrication condition on the surface integrity induced during drag finishing. *Procedia CIRP* **2020**, *87*, 245–250. [CrossRef]
19. Grange, F.; Rech, J.; Kermouche, G. Preparatory Process, by Major Movement, to Develop a Tribofinition Polishing Range. Fr. Patent FR3001170A1, 25 June 2015.
20. International Organization for Standardization. *Geometrical Product Specifications (GPS)—Surface Texture: Areal—Part 2: Terms, Definitions and Surface Texture Parameters*; ISO 25178-2:2012(en); International Organization for Standardization: Geneva, Switzerland, 2012.
21. Lade, P.V.; Nelson, R.B. Modelling the elastic behaviour of granular materials. *Int. J. Numer. Anal. Methods Geomech.* **1987**, *11*, 521–542. [CrossRef]
22. Extended Drucker-Prager Odels. Available online: https://abaqus-docs.mit.edu/2017/English/SIMACAEMATRefMap/simamat-c-druckerprager.htm (accessed on 21 December 2020).
23. Yu, M.-H. Concrete Plasticity. In *Generalized Plasticity*; Springer: Berlin/Heidelberg, Germany, 2006; pp. 155–194. [CrossRef]